UCLouvain

epl

École polytechnique de Louvain

River Bed Profile Evolution Subject to Stochastic Forcing by Migrating Tributaries

Author: **Corentine CHEVILLARD**
Supervisors: **Hervé CAPART, Estelle MASSART**
Readers: **Pierre-Antoine ABSIL, Pierre-Yves GOUSENBOURGER**
Academic year 2023–2024
Master [120] in Mathematical Engineering

Acknowledgements

I would like to thank my supervisors, Prof. Capart Hervé and Prof. Massart Estelle, for their guidance and valuable advice as well as their time.

The National Taiwan University Research Visiting Student Program, without which I would not have been able to go to Taiwan.

I would also like to thank the team of the Civil Engineering Department of the National Taiwan University for their support and advice during my time in Taiwan.

The help of ChatGPT was used for correcting and refining texts to enhance their quality.

Last but not least, many thanks to my family and friends for their support and encouragement.

Abstract

In steep valleys of mountainous regions, civil infrastructures are threatened by changes in the river bed elevation due to rainfall and landslides. The objective of this thesis is to propose a new model of the evolution of the river bed elevation. The elevation changes are modeled with a diffusion equation having a stochastic source term representing the sediment load from tributaries. The migration of the tributaries is represented as a random walk and its properties are derived. To account for rainfall variability, the model is modulated by a hydrologic time. An analytical and a numerical solution are derived for this model. Model calibration is performed using rainfall data and aerial images for the hydrologic time and the parameters of the migrating source.

Contents

Chapter 1

Introduction

In steep valleys of mountainous regions, rainfall and landslides can significantly impact rivers' long profiles, altering riverbed elevations and threatening nearby civil infrastructures. This work examines the Laonong River in Taiwan, which is notable for its steep slopes and high sediment load from tributary rivers. These conditions cause substantial changes in river bed elevation over time, making the Laonong River an ideal subject for this study.

Figure 1.1: River aggradation at Achiba Bridge in September 2019 (Source: photo by Chi-Yao Hung, National Chung-Hsing University)

Figure 1.1 illustrates the effects of typhoons on the river bed, resulting in damage to roads and bridges. The image shows an old bridge almost entirely buried, with only the top of

one of its towers remaining visible. This example highlights the severe impact of sediment deposition and erosion on infrastructure in the area.

The riverbed elevation has changed significantly over the years, as shown in Figure 1.2, where we can see the evolution of a section of the long profile of Laonong River over the years, since 2006, and the position of the two most active tributaries in recent years. The river bed elevation increased by more than 30 meters between 2006 and 2023.

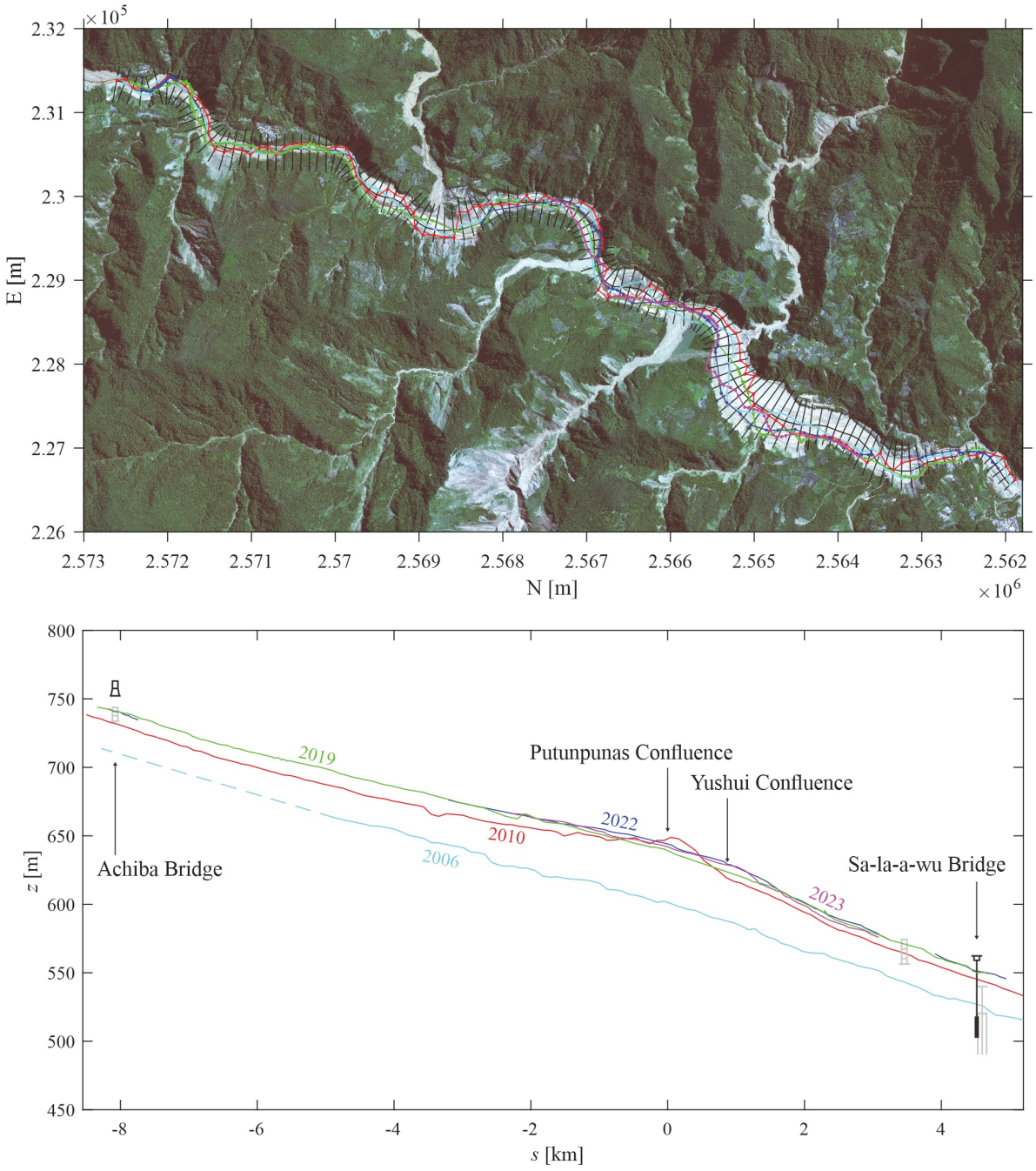

Figure 1.2: Long profile evolution of the Laonong River since 2006 (Source: Morphohydraulics Research Group, National Taiwan University. Figure design by Yuan-Hung Chiu.)

During the first months of my master's thesis, I had the opportunity to spend four months in Taiwan. During this stay, I was able to participate in the field survey to measure the river bed elevation of Laonong River.
This survey was done using a total station, a surveying instrument that can measure angles and distances.

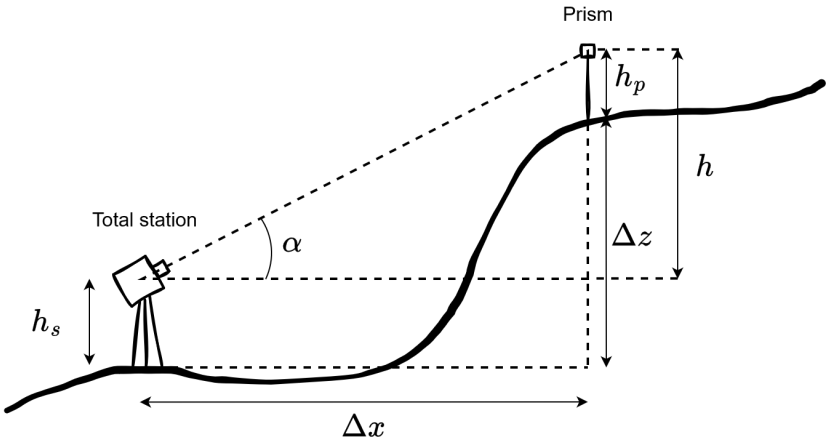

Figure 1.3: Conceptual sketch of a measurement with total station

To evaluate the elevation of the river bed using a total station, we first need to set it up properly. Using GNSS (Global Navigation Satellite Systems), which provides positioning via satellites, we define two control points: the total station emplacement and a control point that serves as zero degrees for the horizontal angle. Then we set horizontally the zero degrees corresponding to the vertical angle.This control point acts as a reference to determine the positions of other points.
To measure the elevation of a point, we use a reflective prism. Figure 1.3 illustrates how the measurement is set up. The total station measures the distance to the prism and the angle from the horizontal axis α. With this information, the horizontal distance Δx and vertical distance h are computed. Knowing the total station height h_s and the prism height h_p, we can derive the difference in elevation between two positions as $\Delta z = h_s + \Delta x - h_p$. From the data collected by the total station, angles and distances, we can determine the position of each point and its elevation, enabling us to derive a long profile of the river bed.

Developing a model to predict the future evolution of river bed elevation could be useful for assessing the risk of damage to infrastructure such as roads and bridges. This model would enable better forecasting of areas at risk of sediment deposition and erosion.

We propose to model the long profile of the river using a diffusion equation, as it has already been done in previous works [1, 2], with a source term representing the sediment load coming from tributaries.
However, the sediment influx is not consistent, it varies with rainfall, with sediment load increasing as rainfall increases. To account for this variability, we introduce a hydrologic time $\tau(t)$ to modulate the rate of change based on rainfall. Following the approach used in [4], we assume gamma-distributed precipitation such that $\Delta\tau = \Delta R/\mu \sim \Gamma(\Delta t/\nu, \nu) > 0$ the hydrologic time $\tau(t)$, where $R(t)$ is the cumulative rainfall, μ is the mean annual

rainfall and ν represents the episodicity.

Figure 1.4: Aerial views of migrating debris flow channels along the surfaces of the Putunpunas (Source: Morphohydraulics Research Group, National Taiwan University).

Besides the hydrologic time, we also need to account for the migration of the tributaries over the years in our source term.
In Figure 1.4, we can observe the evolution of the Putanpunas tributary's position along the main river. The changes in vegetation clearly indicate a movement of the tributary over time. Areas devoid of vegetation mark locations where the tributary has been present once in the last five years. Light vegetation signifies growth over the past five years, indicating the tributary was absent from these areas during this period. Darker, more established vegetation indicates areas where the tributary has not been situated for over ten years.

To model the randomness of the evolution of the position of a tributary, we propose to model it as a random walk. We use the Ornstein-Ulhenbeck process for its mean reverting behavior in order to bound the tributary position. Considering the random walk of the hydrologic time this stochastic process become a Gamma-subordinated Ornstein-Ulhenbeck process, such a process has been studied in earlier works [4, 13].

This master thesis is divided into six chapters. Chapter 2 provides a problem formulation for the river diffusion model and its analytical and numerical solution. Chapter 3 describes the tributary migration model and some properties of this stochastic model. Chapter 4 details the calibration of the source term parameters using collected field data. Chapter 5 combines the river diffusion model with the tributary migration model. Finally, Chapter 6 concludes.

Chapter 2

River diffusion model

In this chapter, we will derive the diffusion equation governing the evolution of the river long profile.

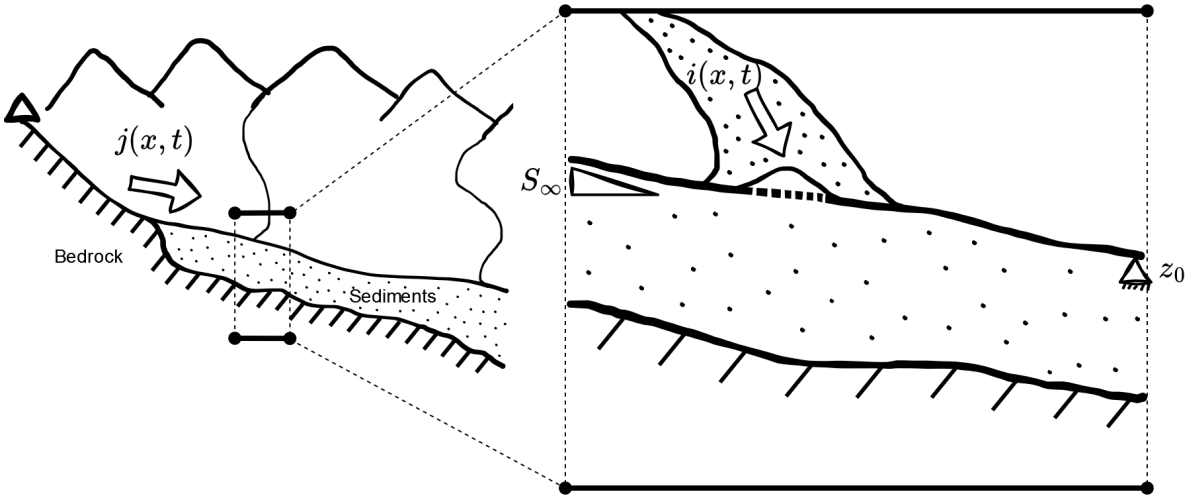

Figure 2.1: Conceptual sketch of the trunk river and a tributary

In Figure 2.1 we can see a conceptual sketch of a river long profile with incoming tributaries, where $j(x,t)$ represents the bed load transport rate of the sediments. On the left side of the figure, a detailed portion shows the boundary conditions and the sediment influx coming from a tributary represented by $i(x,t)$, illustrating its impact on the river's elevation.

2.1 Problem formulation

The evolving elevation $z(x,t)$ of the river bed is supposed to be governed by the Exner equation [12]

$$b\frac{\partial z(x,t)}{\partial t} = -\frac{\partial j(x,t)}{\partial x} + i(x,t) \tag{2.1}$$

where $j(x,t)$ is the bed load transport rate, $i(x,t)$ is the sediment influx from a tributary, x is the curvilinear coordinate measured along the river, and b the river width assumed

to be constant.

We can express the bed load transport rate in the same way as in [1]

$$j(x,t) = KR(t)S(x,t) = -KR(t)\frac{\partial z(x,t)}{\partial x} \tag{2.2}$$

where K is a dimensionless transport coefficient, $R(t)$ is the rainfall, and $S(x,t) = -\frac{\partial z(x,t)}{\partial x}$ is the river slope.

The source term $i(x,t)$ is supposed to be proportional to the rainfall, hence it can be written as

$$i(x,t) = h(x,t)R(t) \tag{2.3}$$

where $h(x,t)$ is source term coefficient.
By substitution of equation (2.2) and (2.3) into the Exner equation (2.1) we obtain the equation of diffusion governing the evolution of the river bed profile, [2]:

$$\frac{\partial z(x,t)}{\partial t} = DR(t)\frac{\partial^2 z(x,t)}{\partial x^2} + \frac{h(x,t)}{b}R(t) \tag{2.4}$$

with $D(t) = \frac{K}{b}$ a time-varying diffusivity.

The coefficient of diffusion depends on the time since the daily rainfall at the upstream station is not constant, to find a valid analytical solution we applied the following change of variable to normalize time dependence in equation (2.4) [1, 5].

$$\tau(t) = \int_{t_0}^{t} R(t')\,dt' \tag{2.5}$$

where τ is the hydrologic time, for which the clock is very slow when the rainfall is low and the clock is very fast when the rainfall is high.

The rainfall can be expressed as

$$\frac{d\tau}{dt} = R(t) > 0. \tag{2.6}$$

Then it follows

$$\frac{\partial z}{\partial t} = \frac{\partial z}{\partial \tau}\frac{d\tau}{dt} = \frac{\partial z}{\partial \tau}R(t). \tag{2.7}$$

From (2.4) we get

$$\frac{\partial z}{\partial t} = \frac{\partial z}{\partial \tau}R(t) = \frac{KR(t)}{b}\frac{\partial^2 z}{\partial x^2} + \frac{h(x,\tau)}{b}R(t). \tag{2.8}$$

By simplification, we obtain the following time independent equation

$$\frac{\partial z(x,\tau)}{\partial \tau} = D\frac{\partial^2 z(x,\tau)}{\partial x^2} + \frac{h(x,\tau)}{b} \tag{2.9}$$

with $D = \frac{K}{b}$ a diffusivity constant.

To be solved, this second order partial differential equation needs two boundary conditions. We choose the upstream boundary to be a constant slope, since upstream the river has reached its long-term equilibrium. For the downstream boundary, we choose a constant elevation, as the level is artificially maintained constant, by removing sediments to keep the river bed below the bridge.

Considering these two boundary conditions, the initial condition and l the length of the section, the problem can be written as follows:

$$\begin{cases} \dfrac{\partial z(x,\tau)}{\partial t} = D\dfrac{\partial^2 z(x,\tau)}{\partial x^2} + \dfrac{h(x,\tau)}{b} \\ z(x,0) = z_0(x) \\ \dfrac{\partial z}{\partial x}(0,\tau) = S_\infty \quad \text{and} \quad z(l,\tau) = z_0(l) \\ 0 \leq x \leq l. \end{cases} \tag{2.10}$$

The slope is created by the water flow and is supposed to be at its steady state, then we can subtract it from the solution [2].

Let $u(x,\tau) = z(x,\tau) - z_0(l)$, the problem become

$$\begin{cases} \dfrac{\partial u(x,\tau)}{\partial t} = D\dfrac{\partial^2 u(x,\tau)}{\partial x^2} + \dfrac{h(x,\tau)}{b} \\ u(x,0) = z_0(x) - z_0(l) = u_0(x) \\ \dfrac{\partial u}{\partial x}(0,\tau) = 0 \quad \text{and} \quad u(l,\tau) = 0 \\ 0 \leq x \leq l. \end{cases} \tag{2.11}$$

Let us derive the solution analytically and then numerically to validate the solution

2.2 Analytical solution

Let $u(x,\tau) = v(x,\tau) + w(x,\tau)$ where $w(x,\tau)$ is a smooth function satisfying only the boundary conditions.

To find the analytical solution, we are going to use Fourier series and the separation of variables.

By separation of variables, we have

$$\begin{aligned} &w(x,\tau) = X(x)T(\tau) \\ &XT' = DTX'' \Rightarrow \frac{T}{DT'} = \frac{X''}{X} = -k^2 \\ &X(x) = A\cos(kx) + E\sin(kx) \quad \text{and} \quad T(\tau) = C\exp\left(-k^2 D\tau\right). \end{aligned}$$

Then from the boundary conditions, we get

$$\begin{aligned}
&X'(x) = -kA\sin(kx) + kE\cos(kx)\\
&X'(0) = kE = 0 \Rightarrow E = 0\\
&X(l) = A\cos(kl) = 0 \quad \Rightarrow k_n = \frac{(2n+1)\pi}{2l} \quad n = 0, 1, 2\ldots\\
&X_n(x) = A_n\cos(k_n x) \quad \text{and} \quad T_n(\tau) = C_n\exp\left(-k_n^2 D\tau\right).
\end{aligned}$$

By the principle of superposition

$$w(x,\tau) = \sum_{n=0}^{\infty} A_n\cos(k_n x)\exp\left(-k_n^2 D\tau\right).$$

Considering the initial solution, we have

$$\begin{aligned}
&u_0(x) = \sum_{n=0}^{\infty} B_n\cos(k_n x) \quad \text{where} \quad B_n = \frac{2}{l}\int_0^l u_0(x)\cos(k_n x)\,dx\\
&w(x,0) = u_0(x)\\
&\sum_{n=0}^{\infty}(A_n - B_n)\cos(k_n x) = 0.
\end{aligned}$$

By cosines orthogonality $A_n = B_n$ and we get

$$A_n = \frac{2}{l}\int_0^l u_0(x)\cos(k_n x)\,dx$$

Hence,

$$w(x,\tau) = \sum_{n=0}^{\infty}\frac{2}{l}\int_0^l u_0(x)\cos(k_n x)\,dx\cos(k_n x)\exp\left(-k_n^2 D\tau\right). \tag{2.12}$$

To find the expression of $v(x,\tau)$ we consider the problem (2.11) with a zero initial condition.

Let us consider the source term and write it as a cosine series

$$h(x,\tau) = \sum_{n=1}^{\infty} F_n(\tau)\cos(k_n x) \quad \text{where} \quad F_n(\tau) = \frac{2}{l}\int_0^l h(x,\tau)\cos(k_n x)\,dx.$$

We can express $v(x,\tau)$ as a cosine series

$$\begin{aligned}
&v(x,\tau) = \sum_{n=0}^{\infty} c_n(\tau)\cos(k_n x)\\
&\frac{\partial v}{\partial \tau} = \sum_{n=0}^{\infty} c_n'(\tau)\cos(k_n x)\\
&\frac{\partial^2 v}{\partial x^2} = \sum_{n=0}^{\infty} c_n(\tau)\left(\cos(k_n x)\right)'' = \sum_{n=0}^{\infty} c_n(\tau)k_n^2\cos(k_n x)\\
&\Rightarrow \sum_{n=0}^{\infty}\left[\left(c_n'(\tau) + Dk_n^2 c_n(\tau) - \frac{F_n(\tau)}{b}\right)\cos(k_n x)\right] = 0.
\end{aligned}$$

By cosines orthogonality, and successively multiplying by $e^{Dk_n^2\tau}$ and integrating from 0 to l we have,

$$\begin{aligned}
&\frac{dc_n(\tau)}{d\tau} + Dk_n^2 c_n(\tau) = \frac{F_n(\tau)}{b}\\
&\frac{dc_n(\tau)}{d\tau}e^{Dk_n^2\tau} + Dk_n^2 c_n(\tau)e^{Dk_n^2\tau} = \frac{F_n(\tau)}{b}e^{Dk_n^2\tau}\\
&\frac{d}{d\tau}\left(e^{Dk_n^2\tau}c_n(\tau)\right) = e^{Dk_n^2\tau}\frac{F_n(\tau)}{b}\\
&e^{Dk_n^2\tau}c_n(\tau) - c_n(0) = \int_0^{\tau} e^{Dk_n^2\tau'}\frac{F_n(\tau')}{b}d\tau'\\
&c_n(\tau) = e^{-Dk_n^2\tau}\int_0^{\tau} e^{Dk_n^2\tau'}\frac{F_n(\tau')}{b}d\tau'.
\end{aligned}$$

Hence,

$$v(x,\tau) = e^{-Dk_n^2\tau}\int_0^{\tau} e^{Dk_n^2\tau'}\frac{2}{lb}\int_0^{l} h(x,\tau')\cos(k_n x)\,dx\,d\tau'\cos(k_n x)\,. \tag{2.13}$$

Adding equations (2.12) and (2.13), the solution of problem (2.11) is

$$\begin{aligned}
u(x,\tau) = &\sum_{n=0}^{\infty}\frac{2}{l}\int_0^{l} u_0(x)\cos(k_n x)\,dx\cos(k_n x)e^{-Dk_n^2\tau}\\
&+\sum_{n=0}^{\infty}\left[\left(\int_0^{\tau} e^{Dk_n^2\tau'}\frac{2}{lb}\int_0^{l} h(x,\tau')\cos(k_n x)\,dx\,d\tau'\right)\cos(k_n x)\,e^{-Dk_n^2\tau}\right].
\end{aligned} \tag{2.14}$$

Hence, the solution of problem (2.10) is

$$\begin{aligned}
z(x,\tau) = &\sum_{n=0}^{\infty}\frac{2}{l}\int_0^{l}(z_0(x) - z_0(l))\cos(k_n x)\,dx\cos(k_n x)e^{-Dk_n^2\tau}\\
&+\sum_{n=0}^{\infty}\left[\left(\int_0^{\tau} e^{Dk_n^2\tau'}\frac{2}{lb}\int_0^{l} h(x,\tau')\cos(k_n x)\,dx\,d\tau'\right)\cos(k_n x)\,e^{-Dk_n^2\tau}\right]\\
&+ z_0(l)
\end{aligned} \tag{2.15}$$

where $k_n = \frac{(2n+1)\pi}{2l}$ for any $n = 0, 1, 2\ldots$

2.3 Numerical solution

A numerical solution can be derived using a forward Euler scheme [10].
We discretize both space and time with Δx the spatial step size, and Δt the temporal step size.

$$Z_i^n = z^h(x_i, t_n) \approx z(x_i, t_n)$$

where i and n are respectively the spatial and temporal indices.

The diffusion equation (2.9) can be written as follows

$$\frac{Z_i^{n+1} - Z_i^n}{\Delta\tau} = D\frac{Z_{i+1}^n - 2Z_i^n + Z_{i-1}^n}{(\Delta x)^2} + \frac{H_i^n}{b}.$$

Let $\beta = D\frac{\Delta\tau}{(\Delta x)^2}$, then the equation become

$$Z_i^{n+1} = Z_i^n + \beta(Z_{i+1}^n - 2Z_i^n + Z_{i-1}^n) + \frac{H_i^n}{b}\Delta\tau. \tag{2.16}$$

Initial condition:

$$Z_i^0 = z_0(x_i).$$

Boundary conditions:

$$\begin{aligned} Z_0^{n+1} &= Z_0^n + \beta(2Z_1^n - 2Z_0' - 2Z_0^n) + \frac{H_i^n}{b}\Delta\tau \\ Z_M^{n+1} &= Z_M^0. \end{aligned}$$

For the forward Euler scheme to be stable, the time step $\Delta\tau$ must satisfy the condition [10]:

$$\Delta\tau \leq \frac{(\Delta x)^2}{2D} \tag{2.17}$$

2.4 Source term

In the diffusion equation (2.9), the source term represents the inflow of sediment. These sediments, coming from tributary rivers along the trunk river, affect the elevation of the riverbed.

This source term can be described as a constant influx coming from a fixed tributary, hence we can model the source term as

$$h(x, \tau) = I\delta(x - X) \tag{2.18}$$

where I is the constant influx coming from the fan to the trunk river, X is the tributary position, and $\delta(x - X)$ is the Dirac delta function centered at position X.

To be more realistic and consider the tributary migration in time, we can model the tributary position as a random walk.

The source term expression becomes

$$h(x,\tau) = I\delta(x - X(\tau)) \tag{2.19}$$

where I is the constant influx coming from the fence to the trunk river, X is the tributary position modeled as a random walk, and τ the hydrologic time, giving the pace of geomorphic evolution with

$$\Delta\tau \sim \Gamma(\frac{\Delta t}{\nu}, \nu) \tag{2.20}$$

2.5 Results and comparison

Let us compare the numerical and analytical solutions without source term and for the simple source term $h(x,\tau) = I\delta(x - X)$.

The analytical solution, equation (2.15), can be written as

$$\begin{aligned}
z(x,\tau) =& z_0(l) + \sum_{n=0}^{\infty} \frac{2}{l} \int_0^l (z_0(x) - z_0(l)) \cos(k_n x)\, dx \cos(k_n x) e^{-Dk_n^2\tau} \\
&+ \sum_{n=0}^{\infty} \left[\left(\int_0^\tau e^{Dk_n^2\tau'} \frac{2}{lb} \int_0^l I\delta(x - X) \cos(k_n x)\, dx\, d\tau' \right) \cos(k_n x)\, e^{-Dk_n^2\tau} \right] \\
=& z_0(l) + \sum_{n=0}^{\infty} \frac{2}{l} \int_0^l (z_0(x) - z_0(l)) \cos(k_n x)\, dx \cos(k_n x) e^{-Dk_n^2\tau} \\
&+ \sum_{n=0}^{\infty} \left[\left(\int_0^\tau e^{Dk_n^2\tau'} \frac{2I}{lb} \cos(k_n X) d\tau' \right) \cos(k_n x)\, e^{-Dk_n^2\tau} \right] \\
=& z_0(l) + \sum_{n=0}^{\infty} \frac{2}{l} \int_0^l (z_0(x) - z_0(l)) \cos(k_n x)\, dx \cos(k_n x) e^{-Dk_n^2\tau} \\
&+ \sum_{n=0}^{\infty} \left[\frac{2I}{lbDk_n^2} (1 - e^{-Dk_n^2\tau}) \cos(k_n X) \cos(k_n x) \right].
\end{aligned} \tag{2.21}$$

For the numerical solution, we have

$$H_i^n = \begin{cases} \frac{I}{\Delta x} & \text{if } x_i - \frac{\Delta x}{2} \le X \le x_i + \frac{\Delta x}{2} \\ 0 & \text{otherwise.} \end{cases} \tag{2.22}$$

The parameter values adopted for the comparison are listed in Table 2.1, and the initial elevation is $z_0(x) = \frac{5}{\sqrt{4\pi 0.1}} e^{\frac{-((x-2)^2}{4 \cdot 0.1}}$ for Figure 2.2a and $z_0(x) = 0$ for Figure 2.2b.
And we use a Monte Carlo simulation to obtain a random walk of τ as a function of t.

Fig.	X [m]	l [m]	b [m]	D [m^2yr^{-1}]	I [m^3yr^{-1}]	Δx [m]	$\Delta\tau$ [yr]	ν [yr]
2.2a	1.33	4	3	0.5	0	0.025	0.0003125	0.10
2.2b	1.33	4	3	0.5	20	0.025	0.0003125	0.10

Table 2.1: Parameter values adopted for the comparisons.

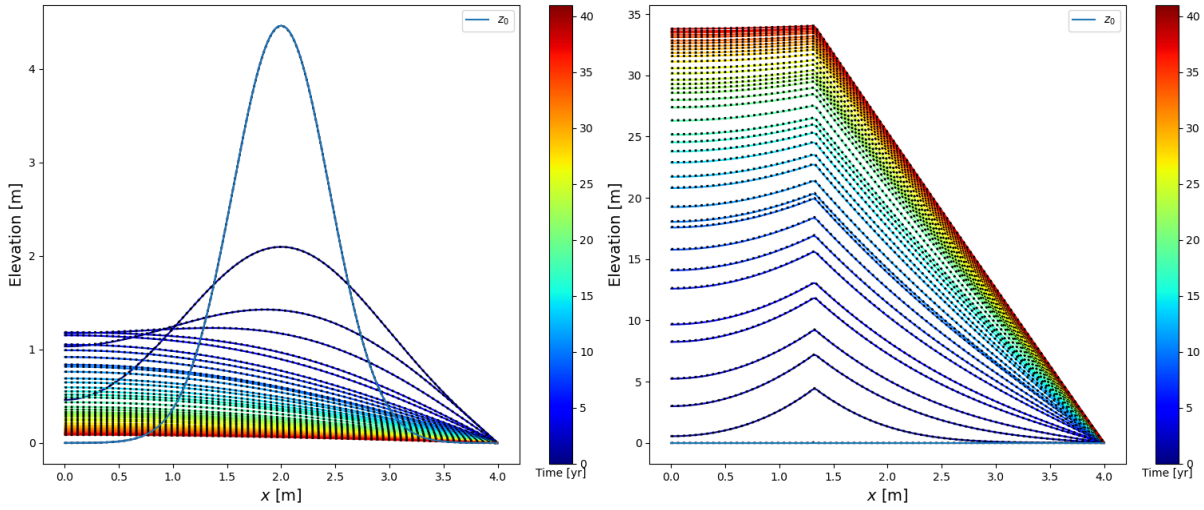

(a) $h(x,\tau) = 0$ (b) $h(x,\tau) = I\delta(x - X)$

Figure 2.2: Comparison of numerical (dots) and analytical (line) results without the source term (a) and with the source term (b).

In figure 2.2, we can see that the numerical (dots) and analytical (line) solutions fit well. Subfigure (a) shows the diffusion of the initial condition without the source term, while subfigure (b) shows the influence of the source term. We can also notice the influence of the hydrologic time, in both subfigure each profile is separated by one year. When two profiles are further apart, it indicates that there has been more rain during that year, resulting in a higher sediment load and, consequently, a greater difference in elevation.

Chapter 3

Tributary migration model

The source term, eq.(2.19), depends on the tributary position. This position is moving over time, due to the environmental fluctuation. This chapter explains how to model the tributary migration and derives the time-evolving properties of the tributary position.

3.1 Model formulation

The tributary position is influenced by some unpredictable environmental factors (rainfalls, landslides...), for that reason the tributary migration over time can be modeled as a random walk.
The Ornstein-Uhlenbeck (OU) process, commonly used in many areas, including physics, can be appropriate to model the migration of the tributary position. Its mean-reverting behavior is suitable for modeling the position over long times and then avoiding unbounded drift. Moreover, this process has well-defined mathematical properties that facilitate the analysis of model behavior and parameter estimation.
The combination of the OU process with the hydrologic time which has a gamma-distributed increment is called a gamma-subordinated OU process (GSOU), such process has been used previously to model random river bed evolution [4]. It allows modeling both the mean-reverting behavior of the position and the irregular event occurrences.

The GSOU process $X(\tau(t))$ is described by the following stochastic differential equation (SDE), by analogy of the SDE of the Standard OU process given in [14]:

$$dX(\tau(t)) = -\lambda(X(\tau(t)) - X_\infty)d\tau(t) + \sigma dW(\tau(t)) \tag{3.1}$$

where λ [yr^{-1}] is the rate at which X reverts to X_∞ [m] the long term mean position, σ [m yr^{-1}] is the volatility, representing the dispersion of the random fluctuations, and $W(\tau(t))$ the Brownian motion, $\tau(t)$ the hydrologic time, giving the pace of geomorphic changes with

$$\Delta\tau \sim \Gamma(\frac{\Delta t}{\nu}, \nu). \tag{3.2}$$

3.2 Hydrologic time evolution

Taken as a function of hydrologic time τ, the process (3.1) is reduced to the classical OU process [4, 14].

We can now derive the solution of this process, and its main properties, such as the time-evolving mean, variance, and autocovariance.

Solution

To obtain the solution of eq. (3.1) we first multiply each side of the equation by $e^{\lambda\tau}$ and then we integrate from 0 to τ

$$\begin{aligned} dX(\tau)e^{\lambda\tau} &= -\lambda(X(\tau) - X_\infty)d\tau e^{\lambda\tau} + \sigma dW(\tau)e^{\lambda\tau} \\ dX(\tau)e^{\lambda\tau} + \lambda X(\tau)e^{\lambda\tau}d\tau &= \lambda X_\infty e^{\lambda\tau}d\tau + \sigma e^{\lambda\tau}dW(\tau) \\ d(X(\tau)e^{\lambda\tau}) &= \lambda X_\infty e^{\lambda\tau}d\tau + \sigma e^{\lambda\tau}dW(\tau) \\ X(\tau)e^{\lambda\tau} - X(0) &= X_\infty e^{\lambda\tau} - X_\infty + \int_0^\tau \sigma e^{\lambda s}dW(s). \end{aligned}$$

This give us the solution

$$X(\tau) = X_\infty + (X(0) - X_\infty)e^{-\lambda\tau} + \sigma\int_0^\tau e^{\lambda(s-\tau)}dW(s). \tag{3.3}$$

Time-evolving mean

The mean position is:

$$\begin{aligned} \mathbb{E}[X(\tau)] &= \mathbb{E}\left[X_\infty + (X(0) - X_\infty)\,e^{-\lambda\tau} + \int_0^\tau \sigma\, e^{\lambda(s-\tau)}dW(s)\right] \\ &= X_\infty + (X(0) - X_\infty)\,e^{-\lambda\tau} \end{aligned} \tag{3.4}$$

where $\mathbb{E}\left[\int_0^\tau e^{\kappa(s-\tau)}dW(s)\right] = 0$ as the expectation of the Itô integral is zero [11, Theorem 3.2.1].

The mean position of the tributary over the hydrologic time is given by $X_\infty + (X(0) - X_\infty)\,e^{-\lambda\tau}$, and the long term mean is X_∞.

Time-evolving variance

$$\begin{aligned}
\mathbb{V}[X(\tau)] &= \mathbb{E}\left[(X(\tau) - \mathbb{E}[X(\tau)])^2\right] \\
&= \mathbb{E}\left[X^2(\tau)\right] - (\mathbb{E}[X(\tau)])^2 \\
&= \mathbb{E}\left[\left(X_\infty + (X(0) - X_\infty)\, e^{-\lambda\tau} + \sigma \int_0^\tau e^{\lambda(s-\tau)} dW(s)\right)^2\right] \\
&\quad - \left(X_\infty + (X(0) - X_\infty)\, e^{-\lambda\tau}\right)^2 \\
&= \left(X_\infty + (X(0) - X_\infty)\, e^{-\lambda\tau}\right)^2 \\
&\quad + 2\sigma \left(X_\infty + (X(0) - X_\infty)\, e^{-\lambda\tau}\right) \mathbb{E}\left[\int_0^\tau e^{\lambda(s-\tau)} dW(s)\right]^{0} \\
&\quad + \sigma^2 \mathbb{E}\left[\left(\int_0^\tau e^{\lambda(s-\tau)} dW(s)\right)^2\right] - \left(X_\infty + (X(0) - X_\infty)\, e^{-\lambda\tau}\right)^2 \\
&= \sigma^2 \mathbb{E}\left[\left(\int_0^\tau e^{\lambda(s-\tau)} dW(s)\right)^2\right].
\end{aligned}$$

Using the Itô isometry property [11, Lemma 3.1.5], it follows that since $e^{s-\tau}$ is bounded and elementary we have $\mathbb{E}\left[\left(\int_0^\tau e^{\lambda(s-\tau)} dW(s)\right)^2\right] = \mathbb{E}\left[\int_0^\tau (e^{\lambda(s-\tau)})^2 ds\right] = \int_0^\tau (e^{\lambda(s-\tau)})^2 ds$, then

$$\mathbb{V}[X(\tau)] = \sigma^2 \int_0^\tau e^{2\lambda(s-\tau)} ds = \frac{\sigma^2}{2\lambda}\left(1 - e^{-2\lambda\tau}\right). \tag{3.5}$$

The variance of the position over the hydrologic time is given by $\frac{\sigma^2}{2\lambda}\left(1 - e^{-2\lambda\tau}\right)$. After a long time, it converges to $\frac{\sigma^2}{2\lambda}$.

Time-evolving autocovariance

$$\begin{aligned}
&\mathrm{Cov}[X(\tau_1), X(\tau_2)] = \mathbb{E}[(X(\tau_1) - \mathbb{E}[X(\tau_1)])(X(\tau_2) - \mathbb{E}[X(\tau_2)])] \\
&= \mathbb{E}\left[\int_0^{\tau_1} \sigma e^{\lambda(s-\tau_1)} dW(s) \int_0^{\tau_2} \sigma e^{\lambda(s-\tau_2)} dW(s)\right] \\
&= \sigma^2 e^{-\lambda(\tau_1+\tau_2)} \mathbb{E}\left[\int_0^{\tau_1} e^{\lambda s} dW(s) \int_0^{\tau_2} e^{\lambda s} dW(s)\right] \\
&= \sigma^2 e^{-\lambda(\tau_1+\tau_2)} \mathbb{E}\left[\left(\int_0^{\min(\tau_1,\tau_2)} e^{\lambda s} dW(s) + \int_{\min(\tau_1,\tau_2)}^{\max(\tau_1,\tau_2)} e^{\lambda s} dW(s)\right) \int_0^{\min(\tau_1,\tau_2)} e^{\lambda s} dW(s)\right] \\
&= \sigma^2 e^{-\lambda(\tau_1+\tau_2)} \mathbb{E}\left[\left(\int_0^{\min(\tau_1,\tau_2)} e^{\lambda s} dW(s)\right)^2 + \int_{\min(\tau_1,\tau_2)}^{\max(\tau_1,\tau_2)} e^{\lambda s} dW(s) \int_0^{\min(\tau_1,\tau_2)} e^{\lambda s} dW(s)\right].
\end{aligned}$$

According to the independence property, the expectation of the product is equal to the product of the expectation, then we can write

$$
\begin{aligned}
&\mathrm{Cov}[X(\tau_1), X(\tau_2)] \\
&= \sigma^2 e^{-\lambda(\tau_1+\tau_2)} \left(\mathbb{E}\left[\left(\int_0^{\min(\tau_1,\tau_2)} e^{\lambda s} dW(s) \right)^2 \right] \right. \\
&\qquad \left. + \mathbb{E}\left[\int_{\min(\tau_1,\tau_2)}^{\max(\tau_1,\tau_2)} e^{\lambda s} dW(s) \right]^{\to 0} \mathbb{E}\left[\int_0^{\min(\tau_1,\tau_2)} e^{\lambda s} dW(s) \right]^{\to 0} \right).
\end{aligned}
$$

Using the Itô isometry and the Itô integral properties used before, we have

$$
\begin{aligned}
\mathrm{Cov}[X(\tau_1), X(\tau_2)] &= \sigma^2 e^{-\lambda(\tau_1+\tau_2)} \mathbb{E}\left[\int_0^{\min(\tau_1,\tau_2)} e^{2\lambda s} ds \right] \\
&= \frac{\sigma^2}{2\lambda} e^{-\lambda(\tau_1+\tau_2)} \left(e^{2\lambda \min(\tau_1,\tau_2)} - 1 \right) \\
&= \frac{\sigma^2}{2\lambda} e^{-\lambda(\tau_1+\tau_2)} \left(e^{\lambda(\tau_1+\tau_2)-\lambda|\tau_1-\tau_2|} - 1 \right) \\
&= \frac{\sigma^2}{2\lambda} \left(e^{-\lambda|\tau_1-\tau_2|} - e^{-\lambda(\tau_1+\tau_2)} \right).
\end{aligned}
\tag{3.6}
$$

The autocovariance over the hydrologic time is given by $\frac{\sigma^2}{2\lambda}\left(e^{-\lambda|\tau_1-\tau_2|} - e^{-\lambda(\tau_1+\tau_2)}\right)$.

For the standard OU process we can easily compare the results with some earlier works [7] and see that they are identical.

3.3 Calendar time evolution

Taken as a function of calendar time t, the process $X(\tau(t))$ becomes the Gamma-subordinated Ornstein-Ulhenbeck (GSOU) process [4, 13] Now let us determine these properties of this more complex GSOU process.

Time-evolving mean

The Brownian motion and the random variable $\tau(t)$ are supposed to be independant. By taking the joint expectation over the Brownian motion and the time Gamma distributed, the mean position is:

$$
\begin{aligned}
\mathbb{E}[X(\tau(t))] &= \mathbb{E}\left[X_\infty + (X(0) - X_\infty)\, e^{-\lambda\tau} + \int_0^\tau \sigma\, e^{\lambda(s-\tau)} dW(s) \right] \\
&= X_\infty + (X(0) - X_\infty)\, \mathbb{E}[e^{-\lambda\tau}] \\
&= X_\infty + (X(0) - X_\infty)\, (\lambda\nu + 1)^{-t/\nu}
\end{aligned}
\tag{3.7}
$$

where $\mathbb{E}\left[\int_0^\tau \sigma\, e^{\kappa(s-\tau)} dW(s)\right] = 0$ as the expectation of the Itô integral is zero [11, Theorem 3.2.1], and $\mathbb{E}[e^{-\lambda\tau}]$ with $\tau \sim \Gamma(\frac{t}{\nu}, \nu)$ is derived as follows

$$\begin{aligned}
\mathbb{E}[e^{-\lambda\tau}] &= \int_0^{+\infty} e^{-\lambda\tau}\, \frac{\nu^{-t/\nu}}{\Gamma(t/\nu)}\, \tau^{t/\nu-1}\, e^{-\tau/\nu} d\tau \\
&= \frac{\nu^{-t/\nu}}{\Gamma(t/\nu)} \int_0^{+\infty} \tau^{t/\nu-1}\, e^{-\tau(\lambda+1/\nu)} d\tau \\
&= \frac{\nu^{-t/\nu}}{\Gamma(t/\nu)} \int_0^{+\infty} \left(\frac{y}{\lambda+1/\nu}\right)^{t/\nu-1} e^{-y}\, \frac{dy}{\lambda+1/\nu} \\
&= \frac{\nu^{-t/\nu}}{\Gamma(t/\nu)}\, (\lambda+1/\nu)^{-t/\nu} \int_0^{+\infty} y^{t/\nu-1}\, e^{-y}\, dy \\
&= \frac{(\nu\lambda+1)^{-t/\nu}}{\Gamma(t/\nu)}\, \Gamma(t/\nu) \\
&= (\lambda\nu+1)^{-t/\nu}
\end{aligned} \tag{3.8}$$

with, in the third line, $y = \tau(\lambda + 1/\nu)$ and $dy = d\tau(\lambda + 1/\nu)$.

The long term mean is X_∞.

Time-evolving variance

Using the previous properties of the Itô integral and the Itô isometry, the time-evolving variance can be derived as

$$
\begin{aligned}
\mathbb{V}[X(\tau(t))] =& \mathbb{E}\left[X^2(\tau)\right] - (\mathbb{E}[X(\tau)])^2 \\
=& \mathbb{E}\left[\left(X_\infty + (X(0) - X_\infty)\, e^{-\lambda\tau}\right)^2\right] \\
&+ \mathbb{E}\left[2\sigma\left(X_\infty + (X(0) - X_\infty)\, e^{-\lambda\tau}\right)\int_0^\tau e^{\lambda(s-\tau)} dW(s)\right] \\
&+ \sigma^2\mathbb{E}\left[\left(\int_0^\tau e^{\lambda(s-\tau)} dW(s)\right)^2\right] \\
&- \left(X_\infty + (X(0) - X_\infty)\,\mathbb{E}\left[e^{-\lambda\tau}\right]\right)^2 \\
=& X_\infty^2 + 2X_\infty\,(X(0) - X_\infty)\,\mathbb{E}\left[e^{-\lambda\tau}\right] + (X(0) - X_\infty)^2\,\mathbb{E}\left[e^{-2\lambda\tau}\right] \\
&+ 2\sigma\left(X_\infty\,\mathbb{E}\left[\int_0^\tau e^{\lambda(s-\tau)} dW(s)\right]^{\to 0} + (X(0) - X_\infty)\,\mathbb{E}\left[\int_0^\tau e^{-\lambda(2\tau - s)} dW(s)\right]^{\to 0}\right) \\
&+ \sigma^2\mathbb{E}\left[\left(\int_0^\tau e^{\lambda(s-\tau)} dW(s)\right)^2\right] \\
&- \left(X_\infty^2 + 2X_\infty\,(X(0) - X_\infty)\,\mathbb{E}\left[e^{-\lambda\tau}\right] + (X(0) - X_\infty)^2\,\mathbb{E}\left[e^{-\lambda\tau}\right]^2\right) \\
=& (X(0) - X_\infty)^2\,\mathbb{E}\left[e^{-2\lambda\tau}\right] + \sigma^2\mathbb{E}\left[\int_0^\tau e^{2\lambda(s-\tau)} ds\right] - (X(0) - X_\infty)^2\,\mathbb{E}\left[e^{-\lambda\tau}\right]^2 \\
=& \sigma^2\mathbb{E}\left[\frac{1}{2\lambda}\left(1 - e^{-2\lambda\tau}\right)\right] + (X(0) - X_\infty)^2\left(\mathbb{E}\left[e^{-2\lambda\tau}\right] - \mathbb{E}\left[e^{-\lambda\tau}\right]^2\right) \\
=& \frac{\sigma^2}{2\lambda}\left(1 - \mathbb{E}\left[e^{-2\lambda\tau}\right]\right) + (X(0) - X_\infty)^2\left(\mathbb{E}\left[e^{-2\lambda\tau}\right] - \mathbb{E}\left[e^{-\lambda\tau}\right]^2\right) \\
=& \frac{\sigma^2}{2\lambda}\left(1 - (2\lambda\nu + 1)^{-t/\nu}\right) + (X(0) - X_\infty)^2\left((2\lambda\nu + 1)^{-t/\nu} - (\lambda\nu + 1)^{-2t/\nu}\right)
\end{aligned}
$$

$$
\mathbb{V}[X(\tau(t))] = \frac{\sigma^2}{2\lambda}\left(1 - (2\lambda\nu + 1)^{-t/\nu}\right) + (X(0) - X_\infty)^2\left((2\lambda\nu + 1)^{-t/\nu} - (\lambda\nu + 1)^{-2t/\nu}\right). \tag{3.9}
$$

The long term variance is $\frac{\sigma^2}{2\lambda}$.

Time-evolving autocovariance

To simplify the notation let $\tau(t_i)) = \tau_i$. The time-evolving autocovariance can be derived as

$$
\begin{aligned}
\mathrm{Cov}\left[X(\tau(t_1)), X(\tau(t_2))\right] &= \mathbb{E}\left[\left(X(\tau_1) - \mathbb{E}\left[X(\tau_1)\right]\right)\left(X(\tau_2) - \mathbb{E}\left[X(\tau_2)\right]\right)\right] \\
&= \mathbb{E}\left[X(\tau_1)X(\tau_2)\right] - \mathbb{E}\left[X(\tau_1)\mathbb{E}\left[X(\tau_2)\right]\right] - \mathbb{E}\left[X(\tau_2)\mathbb{E}\left[X(\tau_1)\right]\right] \\
&\quad + \mathbb{E}\left[\mathbb{E}\left[X(\tau_1)\right]\mathbb{E}\left[X(\tau_2)\right]\right] \\
&= \mathbb{E}\left[X(\tau_1)X(\tau_2)\right] - \mathbb{E}\left[X(\tau_1)\right]\mathbb{E}\left[X(\tau_2)\right]
\end{aligned} \tag{3.10}
$$

Using the same properties of the Itô integral, Itô isometry and independence, than in the standard OU process, the first term is

$$
\begin{aligned}
\mathbb{E}\left[X\left(\tau_1\right)X\left(\tau_2\right)\right] &= \mathbb{E}\left[\left(X_\infty + \left(X(0)-X_\infty\right)e^{-\lambda\tau_1} + \sigma\int_0^{\tau_1} e^{\lambda(0-\tau_1)}dW(s)\right)\right. \\
&\qquad \left.\left(X_\infty + \left(X(0)-X_\infty\right)e^{-\lambda\tau_2} + \sigma\int_0^{\tau_2} e^{\lambda(s-\tau_2)}dW(s)\right)\right] \\
&= \mathbb{E}\left[\left(X_\infty + \left(X(0)-X_\infty\right)e^{-\lambda\tau_1}\right)\left(X_\infty + \left(X(0)-X_\infty\right)e^{-\lambda\tau_2}\right)\right] \\
&\quad + \mathbb{E}\left[\left(X_\infty + \left(X(0)-X_\infty\right)e^{-\lambda\tau_1}\right)\sigma\int_0^{\tau_2} e^{\lambda(s-\tau_2)}dW(s)\right] \\
&\quad + \mathbb{E}\left[\left(X_\infty + \left(X(0)-X_\infty\right)e^{-\lambda\tau_2}\right)\sigma\int_0^{\tau_1} e^{\lambda(s-\tau_1)}dW(s)\right] \\
&\quad + \mathbb{E}\left[\sigma^2 e^{-\lambda(\tau_1+\tau_2)}\int_0^{\tau_1} e^{\lambda s}dW(s)\int_0^{\tau_2} e^{\lambda s}dW(s)\right] \\
&= X_\infty^2 + X_\infty\left(X(0)-X_\infty\right)\left(\mathbb{E}\left[e^{-\lambda\tau_2}\right]+\mathbb{E}\left[e^{-\lambda\tau_1}\right]\right) + \left(X(0)-X_\infty\right)^2\mathbb{E}\left[e^{-\lambda(\tau_1+\tau_2)}\right] \\
&\quad + \sigma^2\mathbb{E}\left[e^{-\lambda(\tau_1+\tau_2)}\left(\int_0^{\min(\tau_1,\tau_2)} e^{\lambda s}dW(s) + \int_{\min(\tau_1,\tau_2)}^{\max(\tau_1\tau_2)} e^{\lambda s}dW(s)\right)\int_0^{\min(\tau_1,\tau_2)} e^{\lambda s}dW(s)\right] \\
&= X_\infty^2 + X_\infty\left(X(0)-X_\infty\right)\left(\mathbb{E}\left[e^{-\lambda\tau_1}\right]+\mathbb{E}\left[e^{-\lambda\tau_2}\right]\right) + \left(X(0)-X_\infty\right)^2\mathbb{E}\left[e^{-\lambda(\tau_1+\tau_2)}\right] \\
&\quad + \sigma^2\mathbb{E}\left[e^{-\lambda(\tau_1+\tau_2)}\left(\int_0^{\min(\tau_1,\tau_2)} e^{\lambda s}dW(s)\right)^2\right] \\
&= X_\infty^2 + X_\infty\left(X(0)-X_\infty\right)\left(\mathbb{E}\left[e^{-\lambda\tau_1}\right]+\mathbb{E}\left[e^{-\lambda\tau_2}\right]\right) + \left(X(0)-X_\infty\right)^2\mathbb{E}\left[e^{-\lambda(\tau_1+\tau_2)}\right] \\
&\quad + \sigma^2\mathbb{E}\left[e^{-\lambda(\tau_1+\tau_2)}\int_0^{\min(\tau_1\tau_2)} e^{2\lambda s}ds\right] \\
&= X_\infty^2 + X_\infty\left(X(0)-X_\infty\right)\left(\mathbb{E}\left[e^{-\lambda\tau_1}\right]+\mathbb{E}\left[e^{-\lambda\tau_2}\right]\right) + \left(X(0)-X_\infty\right)^2\mathbb{E}\left[e^{-\lambda(\tau_1+\tau_2)}\right] \\
&\quad + \frac{\sigma^2}{2\lambda}\mathbb{E}\left[e^{-\lambda(\tau_1+\tau_2)}\left(e^{2\lambda\min(\tau_1,\tau_2)}-1\right)\right] \\
&= X_\infty^2 + X_\infty\left(X(0)-X_\infty\right)\left(\mathbb{E}\left[e^{-\lambda\tau_1}\right]+\mathbb{E}\left[e^{-\lambda\tau_2}\right]\right) + \left(X(0)-X_\infty\right)^2\mathbb{E}\left[e^{-\lambda(2\min(\tau_1,\tau_2)+|\tau_1-\tau_2|)}\right] \\
&\quad + \frac{\sigma^2}{2\lambda}\mathbb{E}\left[e^{-\lambda(2\min(\tau_1,\tau_2)+|\tau_1-\tau_2|)}\left(e^{2\lambda\min(\tau_1,\tau_2)}-1\right)\right] \\
&= X_\infty^2 + X_\infty\left(X(0)-X_\infty\right)\left(\mathbb{E}\left[e^{-\lambda\tau_1}\right]+\mathbb{E}\left[e^{-\lambda\tau_2}\right]\right) + \left(X(0)-X_\infty\right)^2\mathbb{E}\left[e^{-2\lambda\min(\tau_1,\tau_2)}e^{-\lambda|\tau_1-\tau_2|}\right] \\
&\quad + \frac{\sigma^2}{2\lambda}\mathbb{E}\left[e^{-\lambda|\tau_1-\tau_2|}\left(1-e^{-2\lambda\min(\tau_1,\tau_2)}\right)\right] \\
&= X_\infty^2 + X_\infty\left(X(0)-X_\infty\right)\left(\mathbb{E}\left[e^{-\lambda\tau_1}\right]+\mathbb{E}\left[e^{-\lambda\tau_2}\right]\right) + \left(X(0)-X_\infty\right)^2\mathbb{E}\left[e^{-2\lambda\min(\tau_1,\tau_2)}\right]\mathbb{E}\left[e^{-\lambda|\tau_1-\tau_2|}\right] \\
&\quad + \frac{\sigma^2}{2\lambda}\mathbb{E}\left[e^{-\lambda|\tau_1-\tau_2|}\right]\left(1-\mathbb{E}\left[e^{-2\lambda\min(\tau_1,\tau_2)}\right]\right).
\end{aligned}
\tag{3.11}
$$

And the second term is

$$\begin{aligned}\mathbb{E}\left[X(\tau_1)X(\tau_2)\right] = X_\infty^2 + X_\infty\left(X(0)-X_\infty\right)\left(\mathbb{E}\left[e^{-\lambda\tau_1}\right]+\mathbb{E}\left[e^{-\lambda\tau_2}\right]\right)\\ +\left(X(0)-X_\infty\right)^2\mathbb{E}\left[e^{-\lambda\tau_1}\right]\mathbb{E}\left[e^{-\lambda\tau_2}\right].\end{aligned} \tag{3.12}$$

Combining these two terms we get the following time-evolving autocovariance

$$\begin{aligned}&\mathrm{Cov}\left[X(\tau(t_1)),X(\tau(t_2))\right] = \mathbb{E}\left[X(\tau_1)X(\tau_2)\right]-\mathbb{E}\left[X(\tau_1)\right]\mathbb{E}\left[X(\tau_2)\right]\\ &=\frac{\sigma^2}{2\lambda}\mathbb{E}\left[e^{-\lambda|\tau_1-\tau_2|}\right]\left(1-\mathbb{E}\left[e^{-2\lambda\min(\tau_1,\tau_2)}\right]\right)\\ &\quad+\left(X(0)-X_\infty\right)^2\left(\mathbb{E}\left[e^{-2\lambda\min(\tau_1,\tau_2)}\right]\mathbb{E}\left[e^{-\lambda|\tau_1-\tau_2|}\right]-\mathbb{E}\left[e^{-\lambda\tau_1}\right]\mathbb{E}\left[e^{-\lambda\tau_2}\right]\right)\\ &=\frac{\sigma^2}{2\lambda}(\lambda\nu+1)^{-\frac{|t_1-t_2|}{\nu}}\left(1-(2\lambda\nu+1)^{-\frac{\min(t_1,t_2)}{\nu}}\right)\\ &\quad+\left(X(0)-X_\infty\right)^2\left((\lambda\nu+1)^{-\frac{|t_1-t_2|}{\nu}}(2\lambda\nu+1)^{-\frac{\min(t_1,t_2)}{\nu}}-(\lambda\nu+1)^{-\frac{t_1+t_2}{\nu}}\right)\\ &=\frac{\sigma^2}{2\lambda}(\lambda\nu+1)^{-\frac{|t_1-t_2|}{\nu}}\left(1-(2\lambda\nu+1)^{-\frac{\min(t_1,t_2)}{\nu}}\right)\\ &\quad+\left(X(0)-X_\infty\right)^2(\lambda\nu+1)^{-\frac{|t_1-t_2|}{\nu}}\left((2\lambda\nu+1)^{-\frac{\min(t_1,t_2)}{\nu}}-(\lambda\nu+1)^{-\frac{2\min(t_1,t_2)}{\nu}}\right).\end{aligned} \tag{3.13}$$

We can compare our results with some previous works, that have also considered the GSOU process. Our derived mean is identical to the mean derived in [4] and for the variance, our result was different from their own, but it has been corrected recently to the same result [3]. If we compare to another previous work [13], the mean is identical, however the autocovariance (and variance choosing $h = 0$) are different, but it could be due to a misprint since their results seem to be correct in their plots as it coincides with their Monte-Carlo simulations.

3.4 Results and comparison

Discretization

There are different ways to perform Monte-Carlo simulations and observe the model behavior and its properties.
A first and simple method is to discretize the SDE using the Euler scheme. However, after running Monte-Carlo (MC) simulations, it turns out that it does not produce the correct solution properties, even at very fine discretization, hence, an alternative method must be used for the simulation.
Another approach is to use the exact simulation approach of Gillespie [8, 9], however, we first need to adapt it to the GSOU process.

From the solution eq.(3.3) of the SDE, and by adapting by analogy the exact simulation formula of the standard OU process to the GSOU process, given $\Delta\tau_j$, we have

$$X_{j+1} = X_j e^{-\lambda\Delta\tau_j} + z_\infty(1-e^{-\lambda\Delta\tau_j}) + \sigma\sqrt{\frac{1-e^{-2\lambda\Delta\tau_j}}{2\lambda}}N_j(0,1) \tag{3.14}$$

Monte-Carlo results

The parameter values adopted for the comparisons are listed in Table 3.1.

Fig.	$X(0)$ [m]	X_∞ [m]	λ [yr^{-1}]	σ [m yr^{-1}]	ν [yr]
3.1,3.2	0	5	0.2	1.3	2.4
3.3	2	1	1	0.2	2

Table 3.1: Parameter values adopted for the comparisons.

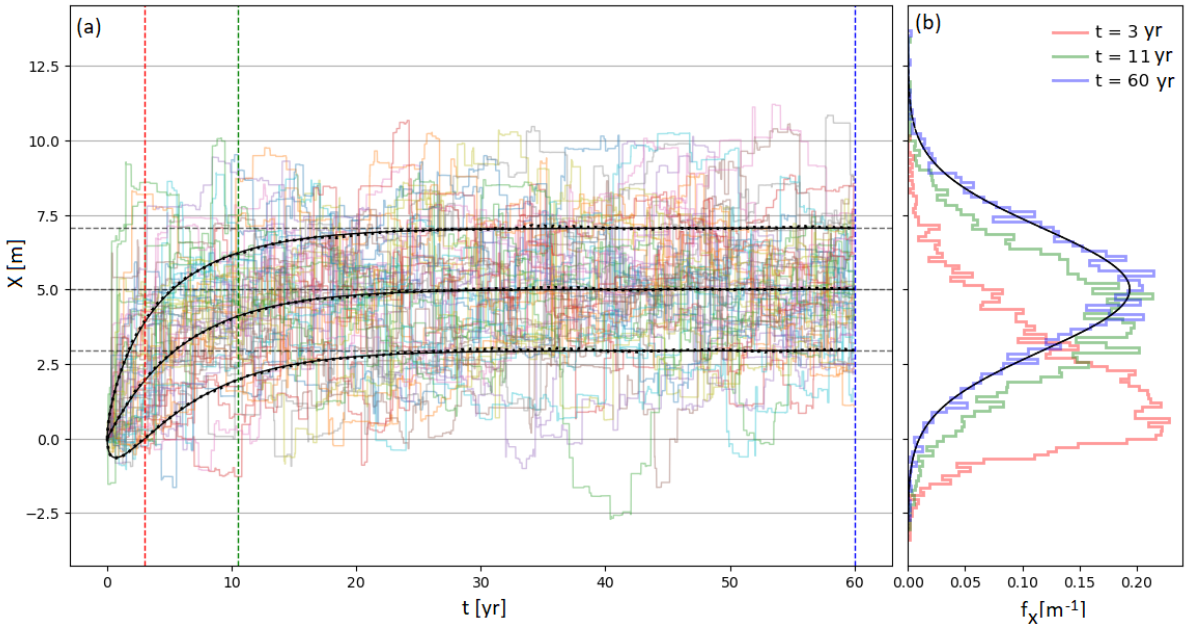

Figure 3.1: (a) 50 paths from $M = 10,000$ Monte-Carlo simulations of tributary position and the evolving mean $\pm$ standard deviation obtained from MC simulations (dots) and from the formulas Eq. (3.7) and Eq. (3.9) (continuous line). (b) The position distribution of the MC simulations at three different times (histogram) and the normal distribution of mean X_∞ and variance $\frac{\sigma^2}{2\lambda}$ (continuous black line).

The position behavior is represented in Figure 3.1a, it shows 50 of the $10,000$ Monte-Carlo simulations, we can see that the derivated properties (continuous line) almost coincide with the properties obtained from MC simulations (dots). Figure 3.1b shows the distribution of the MC simulations for three different times (in red, green and blue), we can see that the long-term distribution tends to follow a normal distribution of mean X_∞ and variance $\frac{\sigma^2}{2\lambda}$ (continuous black line).

In Figure 3.2 we can compare the time-evolving mean and variance, found analytically (continuous line) with the ones resulting from 100,000 Monte-Carlo simulations (dots).

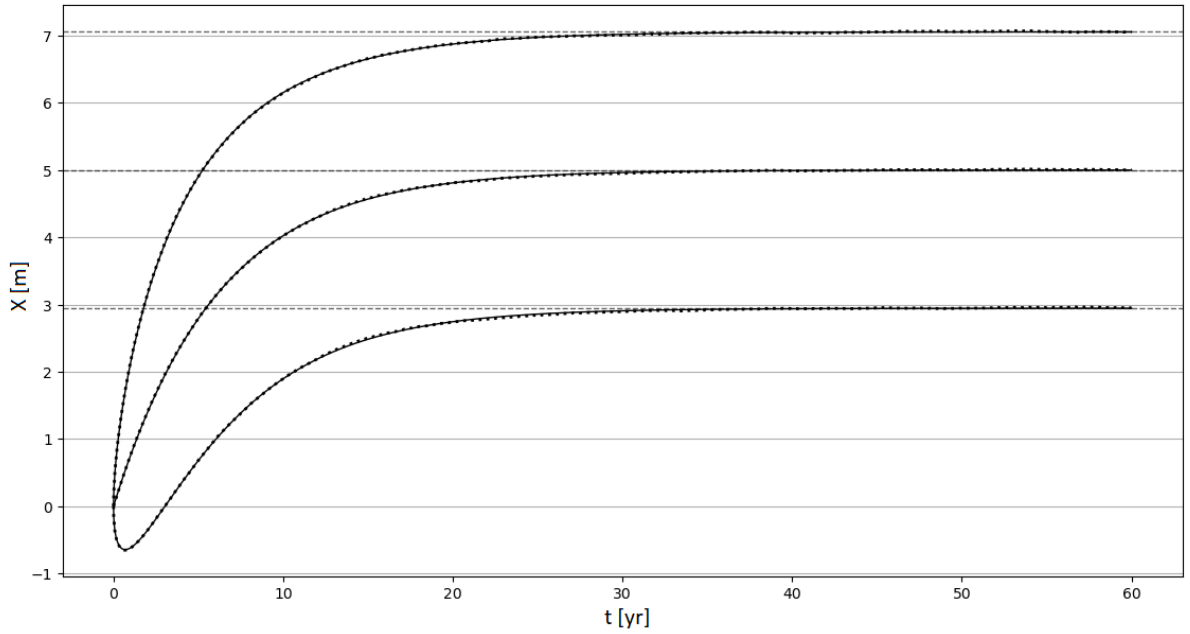

Figure 3.2: Comparison between the evolving mean ± standard deviation obtained from 100,000 MC simulations (dots) and the formulas Eq. (3.7) and Eq. (3.9) (continuous line).

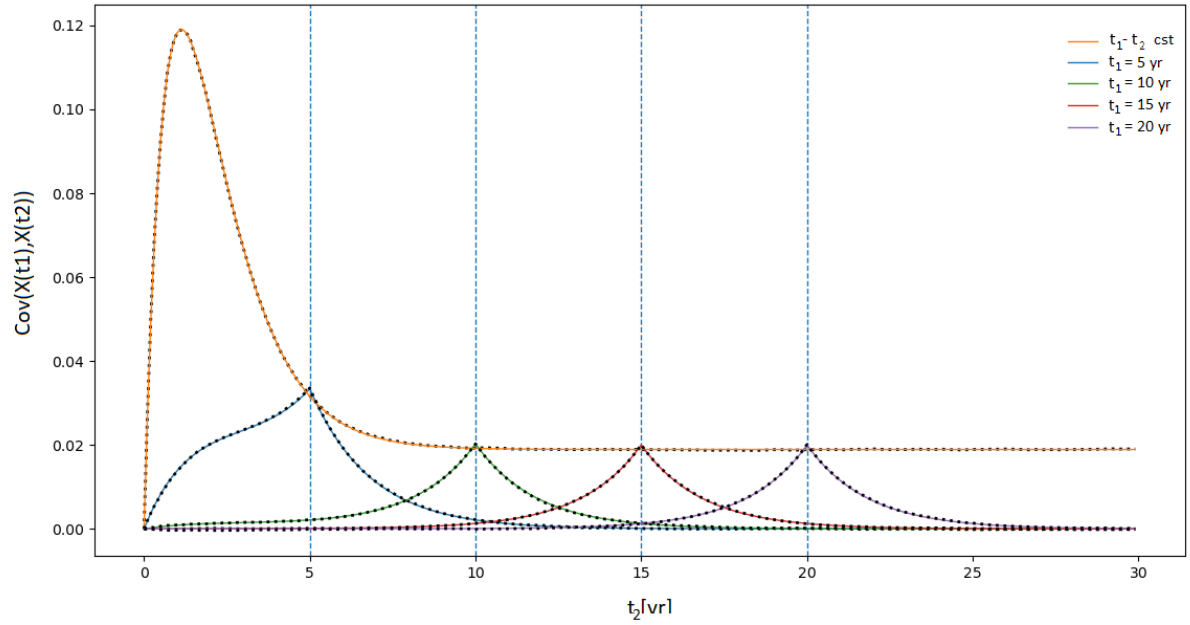

Figure 3.3: Comparison between the evolving covariance obtained from 100,000 MC simulations (dots) and from the formulas Eq. (3.13) (continuous line), with, in orange the evolving covariance for a constant step between t_1 and t_2 and the other colors for a fixed t_1.

The analytical results match well the Monte-Carlo results for both mean and standard deviation.
In Figure 3.3 we can compare the autocovariance found analytically (continuous line) with the ones resulting from 100,000 Monte-Carlo simulations (dots). As for the mean and the variance, the analytical results match well the Monte-Carlo results.

3.5 Discussion

After deriving the time-evolving properties of the tributary position for the calendar time and the hydrologic time, we can see that in both cases the long-term mean and the long-term variance converge respectively to X_∞ and $\frac{\sigma^2}{2\lambda}$. The episodicity ν does not affect the long-term properties of the GSOU process, both OU processes have the same long-term properties, but their convergence rates are different.
And comparing our analytical results with Monte Carlo simulations, we can validate the properties we found for the GSOU process.

Chapter 4

Calibration of the stochastic source term parameters

From the definition and the properties of the tributary position. Let us calibrate the following parameters using field data to apply the model to the Laonong River. We utilize two types of data: rainfall data and aerial images.

X_∞	[m]	Long term position
σ	[m yr^{-1}]	Volatility
ν	[yr]	Episodicity

4.1 Calibration of Gamma distribution parameters from rainfall data

To calibrate the episodicity ν we use the rainfall data from the Tian-Chi rain gauge reported by the Taiwan Water Agency, and we proceed as in [4].

The hydrologic time is assumed to be proportional to the cumulative rainfall $R(t)$ represented in Figure 4.1a, and we assume that the rainfall is gamma-distributed [6].
From the data we can determine the mean annual rainfall $\mu = 3484$ mm/yr, and by fitting the gamma distribution to the yearly rainfall we obtain the episodicity $\nu = 0.103$ yr. To validate the calibration, we can compare the cumulative distribution function (cdf) obtained with the calibrated parameters and the empirical cdf. To find the empirical cdf, we sort the rainfall data in ascending order and for each data we compute $(i - 0.5)/N$ where i is the rank and N is the number of data. In Figure 4.1b we can see that they fit well.

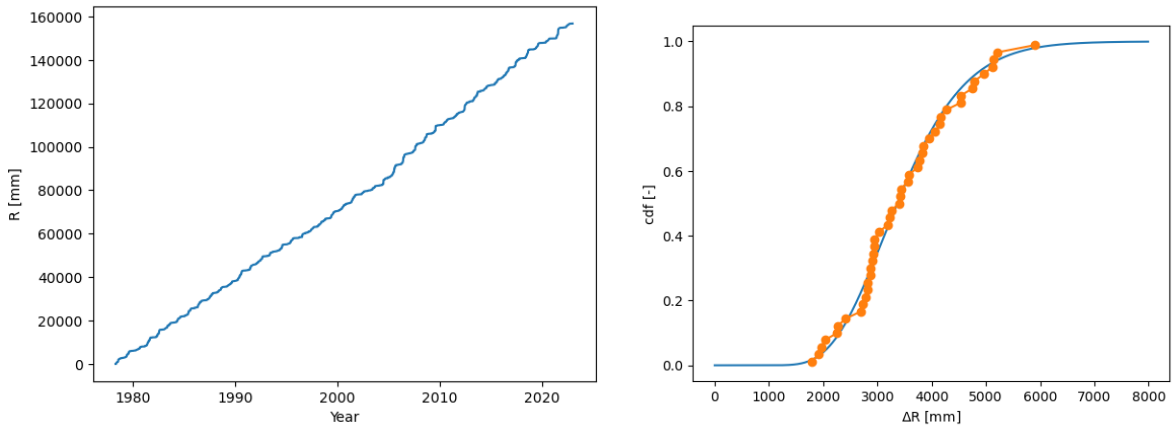

(a) (b)

Figure 4.1: (a) Cumulative rainfall at Tian-Chi rain gauge. (b) Comparison between the fitted cumulative distribution function for the Gamma distribution (line) and empirical cumulative distribution (dots).

4.2 Calibration of GSOU process parameters from aerial images

For the positions of the tributaries, we use aerial images of Laonong River provided by the Forestry and Nature Conservation Agency, and EOSDA LandViewer.

4.2.1 Data processing

To obtain the coordinates of the tributary positions, we use QGIS software. In each image, we try to identify the positions of Putanpunas and Yushui tributaries, which have been the most active recently, though not simultaneously. However, approximately 30% of the images do not clearly show the tributary positions due to poor image quality, resulting in some gaps in our data collection. Figure 4.2 shows an aerial image from the Forestry and Nature Conservation Agency, with tributary positions marked at different times between 2005 and 2021.
From the coordinates obtained at different times, we can plot the evolution of the tributaries positions over time in Figure 4.3.

To calibrate the parameters of the OU process, we need to reduce the dimensionality of our data. First, we fit a line representing the trunk river using linear regression. Then, we project the tributary position points onto this line using the least squares approach. By maintaining the distance between each successive projected position over time, we can plot the evolution of the tributary positions in Figure 4.4.

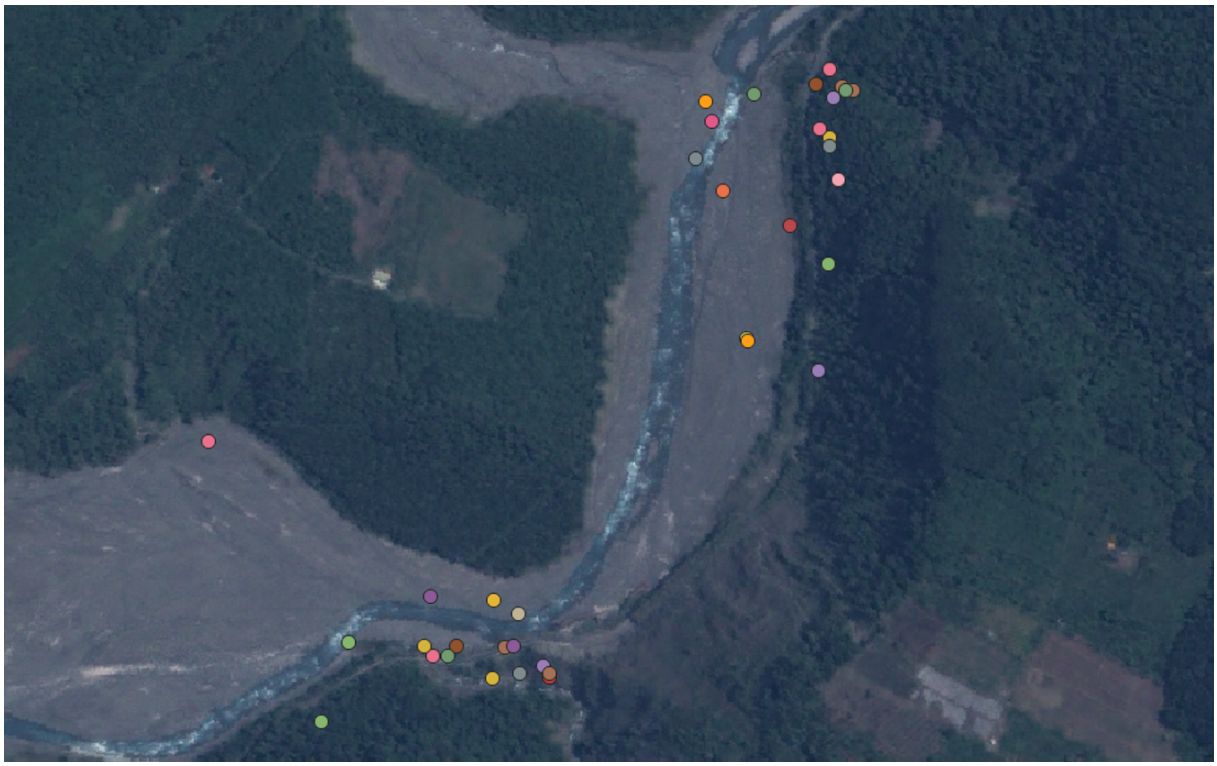

Figure 4.2: Laonong River on July 10th 2005, with coming tributaries position. (Source: Forestry and Nature Conservation Agency.)

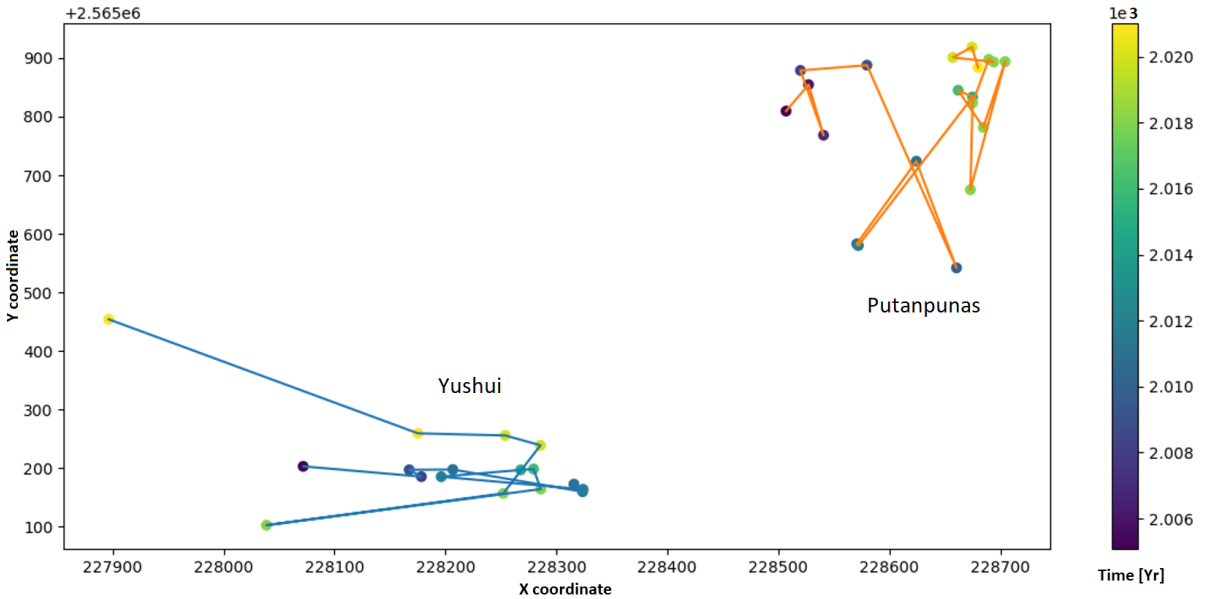

Figure 4.3: Evolution of the tributaries position between 2005 and 2021

4.2.2 Calibration

Let us suppose that the positions are normally distributed, as the OU process tends to a normal distribution over a long period. This allows us to find σ, the volatility coefficient, and X_∞, the long term mean position, for each tributary. For Putanpunas tributary, we

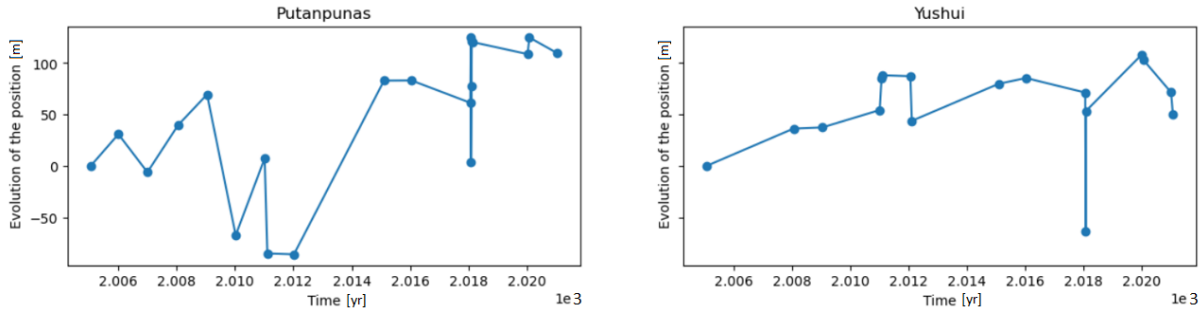

Figure 4.4: Evolution of the tributaries position between 2005 and 2021 after the reduction of dimension.

obtain $X_{\infty PT} = 46.1$ m and $\sigma_{PT} = 67.8$ m, and for Yushui tributary, we find $X_{\infty YS} = 58.3$ m and $\sigma_{YS} = 40.6$ m.

To validate the results, we proceed in the same way as we have done for the gamma distribution parameters. We use the cdf for the comparison as the number of data is small we cannot compare the distribution with a histogram.

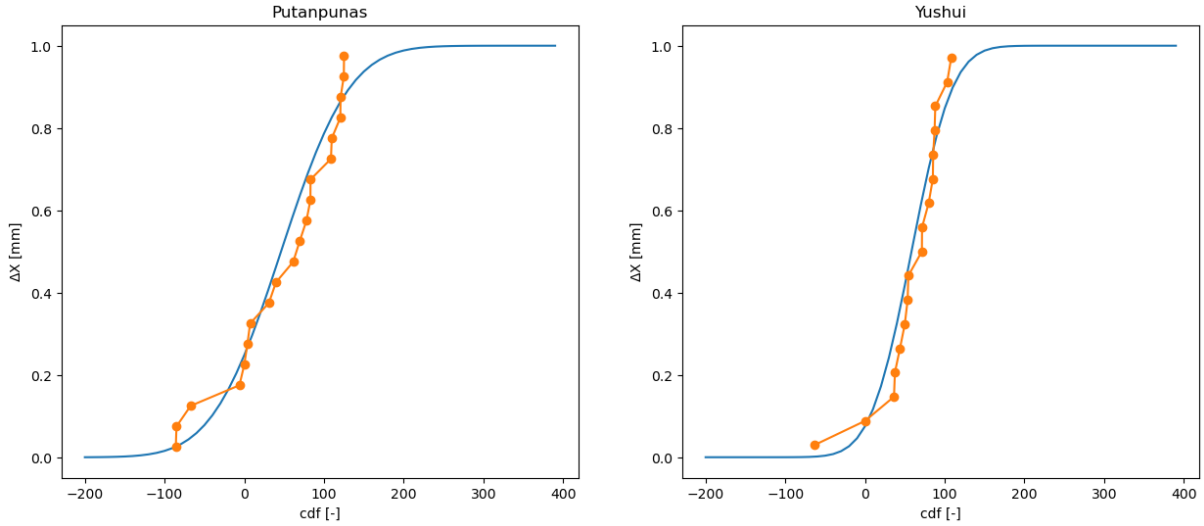

Figure 4.5: Comparison between the fitted cumulative distribution function (line) and empirical cumulative distribution (dots).

In Figure 4.5 we can see that the assumed distributions fit the data reasonably well. While it is not as obvious as it is for the cumulative rainfall, it fits them enough to not reject the hypothesis.

All calibrated values of the parameters are listed in Table 4.1.

Tributary	X_∞ [m]	λ [yr^{-1}]	σ [m yr^{-1}]	ν [yr]
Putanpunas	46.1	0.59	67.8	0.103
Yushui	58.3	1.05	40.6	0.103

Table 4.1: Calibrated values of the parameters.

Chapter 5

Joint model

Let us combine the diffusion model, equation (2.9) with the source term model, equation (2.19). This results in the following equation:

$$\frac{\partial z(x,\tau)}{\partial \tau} - D\frac{\partial^2 z(x,\tau)}{\partial x^2} = \frac{I}{b}\delta(x - X(\tau)). \tag{5.1}$$

5.1 Numerical solution

As we saw in Chapter 2 the numerical solution fits well with the analytical solution. Therefore, for simplicity, we will use the numerical solution to simulate the long profile evolution.

For equation (5.1), the solution is:

$$Z_i^{n+1} = Z_i^n + \beta(Z_{i+1}^n - 2Z_i^n + Z_{i-1}^n) + \frac{H_i^n}{b}\Delta\tau. \tag{5.2}$$

Initial condition:

$$Z_i^0 = z_0(x_i).$$

Boundary conditions:

$$\begin{aligned} Z_0^{n+1} &= Z_0^n + \beta(2Z_1^n - 2Z_0' - 2Z_0^n) + \frac{H_i^n}{b}\Delta\tau \\ Z_M^{n+1} &= Z_M^0. \end{aligned}$$

With

$$H_i^n = \begin{cases} \frac{I}{\Delta x} & \text{if } x_i - \frac{\Delta x}{2} \leq X_n \leq x_i + \frac{\Delta x}{2} \\ 0 & \text{otherwise.} \end{cases} \tag{5.3}$$

5.2 Simulations

The parameters adopted for the simulations are listed in Table 5.1, some of these parameters were calibrated in 4, while the others have been chosen arbitrarily.

Tributary	X_0 [m]	X_∞ [m]	λ [yr^{-1}]	σ [m yr^{-1}]	ν [yr]
Putanpunas	8×10^3	8.0461×10^3	0.59	67.8	0.103
Yushui	8.4×10^3	8.4583×10^3	1.05	40.6	0.103

Tributary	l [m]	b [m]	D [m^2yr^{-1}]	I [m^3yr^{-1}]	Δx [m]	$\Delta\tau$ [yr]
Putanpunas	12×10^3	3	10	20	1	3.125×10^{-4}
Yushui	12×10^3	3	10	20	1	3.125×10^{-4}

Table 5.1: Parameter values.

We consider a section similar to the one visible in Figure 1.2, and set the initial condition equal to 0.
First, we will simulate the evolution of the long profile in the case where the two tributaries are not active during the same period. Then we will examine what happens if the two tributaries were active simultaneously.
To simulate the evolution of the tributary position, we use equation (3.14). And we use Monte Carlo simulation to obtain a random walk of τ in funtion of t.

5.2.1 Putanpunas tributary

Figure 5.1 shows a possible evolution of Putanpunas tributary position over 40 years. Figure 5.2 illustrates the associated evolution of the elevation.

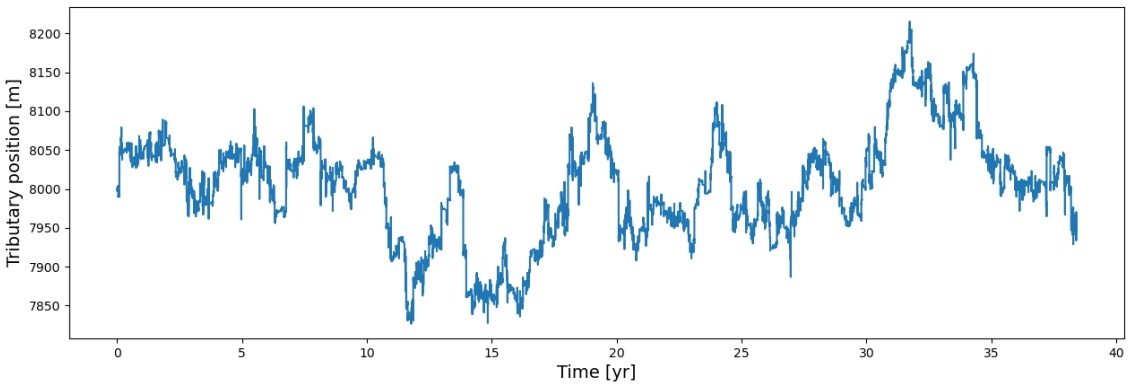

Figure 5.1: Evolution of Putanpunas tributary position

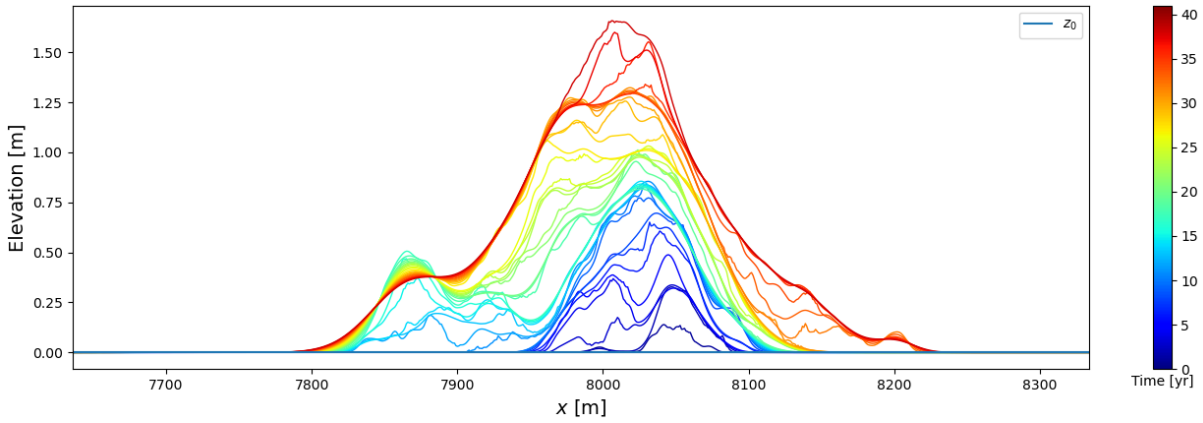

Figure 5.2: Evolution of the long profile at Putanpunas tributary

5.2.2 Yushui tributary

Figure 5.3 shows a possible evolution of Yushui tributary position, over 40 years.

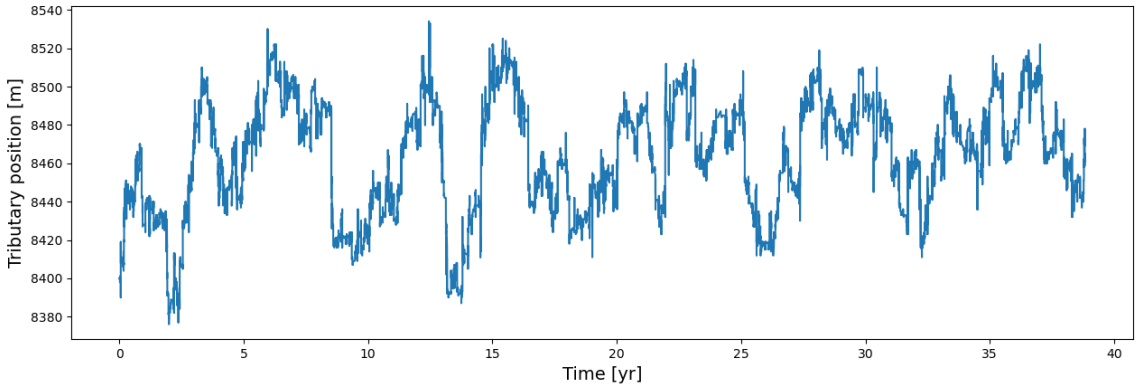

Figure 5.3: Evolution of Yushui tributary position

Figure 5.4 illustrates the associated evolution of the elevation.

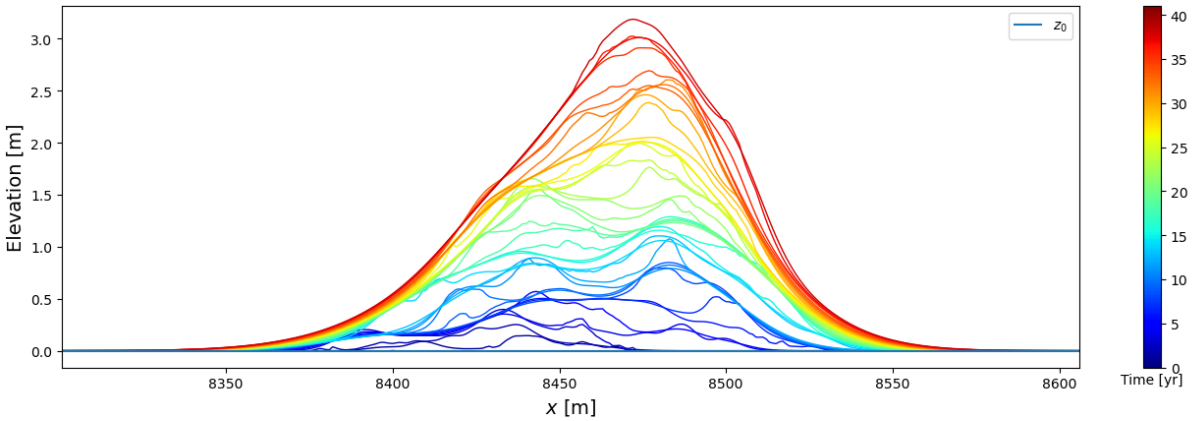

Figure 5.4: Evolution of the long profile at Yushui tributary

5.2.3 Both tributaries active simultaneously

Figure 5.5 shows the evolution of both tributaries position, over 40 years, with a new Monte Carlo simulation to obtain the random walk of τ as a function of t.

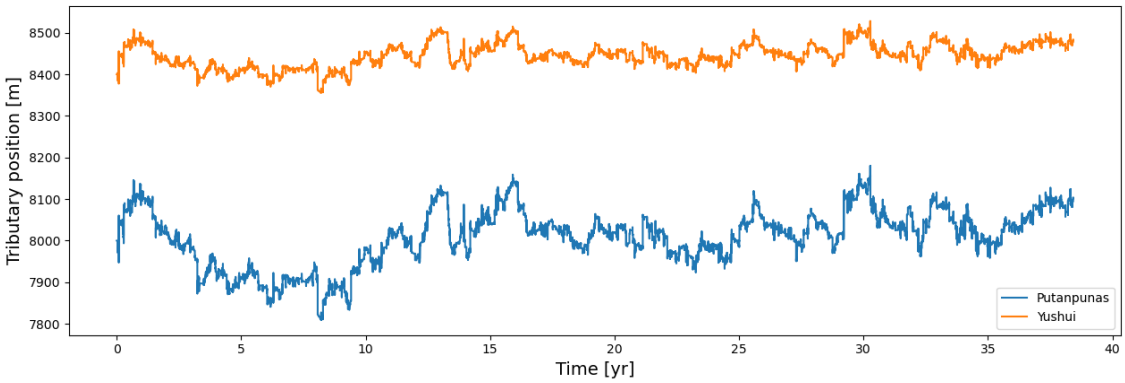

Figure 5.5: Evolution of Putanpunas and Yushui tributary position

Figure 5.6 illustrates the associated evolution of the elevation.

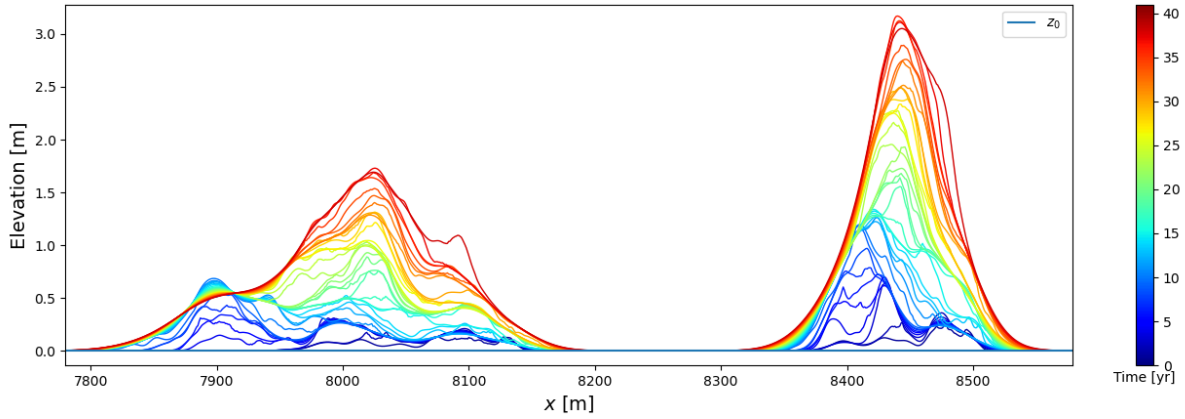

Figure 5.6: Evolution of the long profile with both tributaries active at the same time

5.3 Discussion

Comparing Figure 5.2 and Figure 5.4 and both tributaries in Figure 5.6, we can see that the evolution of the long profile is quite different between the two tributaries. At Putanpunas tributary, the diffusion is wider, and the elevation is lower compare to Yushui tributary. This can be attributed to both the reversion rate λ and the volatility σ, which are respectively greater and lower for Yushui tributary, resulting in less variation in its position, as shown in Figure 5.5.

We can see in Figure 5.6 that for both tributaries the evolution of the elevation is similar to the evolution of the elevation when they are active individually Figure 5.2 and Figure 5.4. This similarity holds even though different Monte Carlo simulations were used to

obtain the random walk of τ as a function of t. Additionally, we can see that for the adopted parameters, the two tributaries are far enough apart to be considered distinct sources.

Chapter 6

Conclusion

This thesis aimed to develop a comprehensive model for predicting the future evolution of river bed elevation, a critical factor in assessing the risk of damage to infrastructure such as roads and bridges. The model, based on a diffusion equation, incorporates a source term representing the sediment load from tributaries, modulated by a hydrologic time $\tau(t)$ to account for rainfall variability.

The hydrologic time, with an increment assumed to follow a gamma distribution, accurately represents the increase in sediment load with increasing rainfall. This approach, inspired by [4], has been successful in modeling the impact of rainfall on sediment influx.

In addition, the model also takes into account the migration of tributaries over time. The migration was modeled as a random walk using the Ornstein-Uhlenbeck process (OU), which provided a bounded and mean-reverting behavior for the tributary position. This approach, combined with the random walk of the hydrologic time, resulted in a Gamma-subordinated Ornstein-Uhlenbeck process (GSOU), as studied in earlier works [4, 13].

The model was calibrated using rainfall data and aerial images of the Laonong River. The combination of the river diffusion model with the tributary migration model provided a comprehensive tool for predicting the future evolution of the river bed elevation.

Future work could focus on calibrating the remaining model parameters for better accuracy and exploring other factors that could influence the sediment load and tributary migration. The long term mean could be derived from the analytical solution and compared to the long term mean of the numerical solution. The model could also be extended to other regions and river systems, further validating its applicability and efficiency.

In conclusion, this thesis could help in predicting river bed elevation, offering a useful tool for assessing infrastructure risk and taking steps to protect and maintain essential structures.

Bibliography

[1] Hervé Capart. Analytical solutions for gradual dam breaching and downstream river flooding. *Water Resources Research*, 49(4):1968–1987, 2013.

[2] Hervé Capart, Jammie PC Hsu, Steven YJ Lai, and Meng-Long Hsieh. Formation and decay of a tributary-dammed lake, Laonong River, Taiwan. *Water Resources Research*, 46(11), 2010.

[3] Tzu-Yin Kasha Chen, Corentine Chevillard, Chi-Yao Hung, Yu-Chou Chiang, Meng-Long Hsieh, and Hervé Capart. Corrigendum to "a stochastic model of geomorphic risk due to episodic river aggradation and degradation" [Engineering Geology 309 (2022) 106845]. *Engineering Geology*, 333:107504, 2024.

[4] Tzu-Yin Kasha Chen, Chi-Yao Hung, Yu-Chou Chiang, Meng-Long Hsieh, and Hervé Capart. A stochastic model of geomorphic risk due to episodic river aggradation and degradation. *Engineering Geology*, 309:106845, 2022.

[5] John Crank. *The mathematics of diffusion*. Oxford University Press, 1979.

[6] Peter S Eagleson. Climate, soil, and vegetation: 2. The distribution of annual precipitation derived from observed storm sequences. *Water Resources Research*, 14(5):713–721, 1978.

[7] Crispin W Gardiner et al. *Handbook of stochastic methods*, volume 3. Springer Berlin, 1985.

[8] Daniel T Gillespie. *Markov processes: an introduction for physical scientists*. Elsevier, 1991.

[9] Daniel T Gillespie. Exact numerical simulation of the Ornstein-Uhlenbeck process and its integral. *Physical review E*, 54:2084–2091, 1996.

[10] Vincent Legat. *Mathématiques et méthodes numériques*. 2019.

[11] Bernt Øksendal. *Stochastic differential equations*. Springer, 2003.

[12] Chris Paola and Vaughan R Voller. A generalized Exner equation for sediment mass balance. *Journal of Geophysical Research: Earth Surface*, 110(F4), 2005.

[13] Paula Poczynek, Piotr Kruczek, and Agnieszka Wyłomańska. Ornstein-Uhlenbeck process delayed by Gamma subordinator. In *Cyclostationarity: Theory and Methods–IV: Contributions to the 10th Workshop on Cyclostationary Systems and Their Applications, February 2017, Grodek, Poland 10*, pages 147–165. Springer, 2020.

[14] George E Uhlenbeck and Leonard S Ornstein. On the theory of the Brownian motion. *Physical review*, 36:823–841, 1930.

UNIVERSITÉ CATHOLIQUE DE LOUVAIN
École polytechnique de Louvain
Rue Archimède, 1 bte L6.11.01, 1348 Louvain-la-Neuve, Belgique | **www.uclouvain.be/epl**